Biomaterials Advances 152 (2023) 213523

Contents lists available at ScienceDirect

Biomaterials Advances

journal homepage: www.journals.elsevier.com/materials-science-and-engineering-c

Antibacterial PLA/Mg composite with enhanced mechanical and biological performance for biodegradable orthopedic implants

Hyun Lee [a,b], Da-Young Shin [c], Yuhyun Na [a,b], Ginam Han [a,b], Joodeok Kim [d], Nahyun Kim [a,b], Seo-Jun Bang [a,b], Hyeong Seok Kang [a,b], SeKwon Oh [e], Chang-Bun Yoon [f], Jungwon Park [g,h,i,j], Hyoun-Ee Kim [c], Hyun-Do Jung [a,b], Min-Ho Kang [a,b,*]

[a] Department of Biomedical-Chemical Engineering, The Catholic University of Korea, 43 Jibong-ro, Bucheon-si, Gyeonggi-do 14662, Republic of Korea
[b] Department of Biotechnology, The Catholic University of Korea, 43 Jibong-ro, Bucheon-si, Gyeonggi-do 14662, Republic of Korea
[c] Department of Materials Science and Engineering, Seoul National University, Seoul 08826, Republic of Korea
[d] School of Chemical and Biological Engineering, Seoul National University, Seoul 08826, Republic of Korea
[e] Research Institute of Advanced Manufacturing & Materials Technology, Korea Institute of Industrial Technology, Incheon 21999, Republic of Korea
[f] Department of Advanced Materials Engineering, Tech University of Korea, Siheung-si 15073, Republic of Korea
[g] School of Chemical and Biological Engineering, Institute of Chemical Processes, Seoul National University, Seoul 08826, Republic of Korea
[h] Center for Nanoparticle Research, Institute of Basic Science (IBS), Seoul 08826, Republic of Korea
[i] Institute of Engineering Research, College of Engineering, Seoul National University, Seoul 08826, Republic of Korea
[j] Advanced Institutes of Convergence Technology, Seoul National University, Suwon-si 16229, Republic of Korea

ARTICLE INFO

Keywords:
Polylactic acid (PLA)
Magnesium (Mg)
Biodegradable composite
Antibacterial effect
Orthopedic applications

ABSTRACT

Biodegradability, bone-healing rate, and prevention of bacterial infection are critical factors for orthopedic implants. Polylactic acid (PLA) is a good candidate biodegradable material; however, it has insufficient mechanical strength and bioactivity for orthopedic implants. Magnesium (Mg), has good bioactivity, biodegradability, and sufficient mechanical properties, similar to that of bone. Moreover, Mg has an inherent antibacterial property via a photothermal effect, which generates localized heat, thus preventing bacterial infection. Therefore, Mg is a good candidate material for PLA composites, to improve their mechanical and biological performance and add an antibacterial property. Herein, we fabricated an antibacterial PLA/Mg composite for enhanced mechanical and biological performance with an antibacterial property for application as biodegradable orthopedic implants. The composite was fabricated with 15 and 30 vol% of Mg homogeneously dispersed in PLA without the generation of a defect using a high-shear mixer. The composites exhibited an enhanced compressive strength of 107.3 and 93.2 MPa, and stiffness of 2.3 and 2.5 GPa, respectively, compared with those of pure PLA which were 68.8 MPa and 1.6 GPa, respectively. Moreover, the PLA/Mg composite at 15 vol% Mg exhibited significant improvement of biological performance in terms of enhanced initial cell attachment and cell proliferation, whereas the composite at 30 vol% Mg showed deteriorated cell proliferation and differentiation because of the rapid degradation of the Mg particles. In turn, the PLA/Mg composites exerted an antibacterial effect based on the inherent antibacterial property of Mg as well as the photothermal effect induced by near-infrared (NIR) treatment, which can minimize infection after implantation surgery. Therefore, antibacterial PLA/Mg composites with enhanced mechanical and biological performance may be a candidate material with great potential for biodegradable orthopedic implants.

1. Introduction

Orthopedic implants are applied to support a damaged bone or substitute missing bone tissues [1–4]. The bone-healing rate of orthopedic implants is a critical factor for accelerating the recovery of patients and preventing the bone tissue destruction that may occur with insufficient healing [3,5]. In addition, the management of infectious bone defects has arisen as a great challenge in orthopedics, as infections

* Corresponding author at: Department of Biomedical-Chemical Engineering, The Catholic University of Korea, 43 Jibong-ro, Bucheon-si, Gyeonggi-do 14662, Republic of Korea.
E-mail address: mhkang@catholic.ac.kr (M.-H. Kang).

https://doi.org/10.1016/j.bioadv.2023.213523
Received 31 March 2023; Received in revised form 29 May 2023; Accepted 12 June 2023
Available online 13 June 2023

can impede local tissue and bone regeneration, thus delaying the healing process [6–8]. In particular, large bone defects pose a high risk of infection and, at the same time, are more challenging, with greater exposure to pathogens and open wounds, which are frequently present in the vicinity of orthopedic implants (such as internal fixation devices), contributing to higher infection rates [6,9]. Moreover, bacterial colonization can impair the functionality of osteogenic cell, leading to delayed bone union or chronic osteomyelitis [10–13].

The conventional methods used for managing bone defects involve the control of infection and the restoration of the damaged bone [14]. However, the main concern is the control of infection, and the present clinical treatments include excision of the infected site, systemic administration of antibiotics, and usage of spacers infused with antibiotics for implantation [15–17]. However, delivering effective local antibiotic concentrations is challenging because of complications such as infection-induced vascular destruction and osteonecrosis [14]. Although localized delivery of antibiotics is possible with antibiotic-impregnated spacers, membrane induction may be needed for bone grafting and the spacers have to be removed in a secondary surgery after about 6 weeks [18–20]. Bone grafting or bone transport techniques may be utilized for bone defect repair only after the infection is under control. Autogenous bone, which is the most effective bone graft, has issues such as donor bone mass inadequacy and donor site complications [21]. Allogeneic grafts carry the risk of infection and immune rejection [22]. Although distraction osteogenesis-based bone transport is effective, it is a long process, typically lasting >10 months [23,24]. The traditional treatment with repetitive surgery–healing cycles is also time consuming, has numerous drawbacks, and is a burden to patients. As a result, developing bone substitutes that promote bone growth and prevent bacterial growth in a single step without requiring additional surgery would be a significant clinical achievement.

The use of hyperthermia in antibacterial therapies draws inspiration from fever, which is a sign of immune activation against invading pathogens [25,26]. Recently, non-invasive antibacterial treatments using photothermal therapy via near-infrared (NIR) irradiation have gained popularity [27–29]. The NIR wavelength ranges from 700 to 1300 nm, and it can achieve targeted photothermal treatment while minimizing the heating effects on normal tissues without the photothermal agents [30–33]. Photothermal therapy is a promising antibacterial strategy because of its ease of use and on-demand response [34,35]. By applying photothermal agents to bone implants, NIR irradiation can be used to generate localized heat, which can ablate peri-implant pathogenic bacteria [28].

Metallic biomaterials are applied as orthopedic implant materials because of their excellent mechanical strength, which can withstand the loading pressures, and good biocompatibility [37–39]. However, a stress shielding effect can be triggered by the high mismatch between the elastic modulus of the metallic implant and that of the bone, which can result in the loosening of the implant from the surrounding bone tissue [40–44]. In addition, a second surgical intervention for the removal of the implant after full healing is achieved is necessary for non-biodegradable metallic biomaterials, which can be an additional burden to the patients. Therefore, biodegradable materials can be used as an alternative to non-biodegradable metallic materials, thus eliminating the necessity for secondary surgery [45–47]. Biodegradable polymers, including polylactic acid (PLA), poly(ι-lactide) (PLLA), poly (ε-caprolactone) (PCL), polyglycolide (PGA), and poly(lactide-co-glycolide) (PLGA), have been applied for the preparation of various biomedical implants [48–51]. Among the biodegradable polymers with elastic moduli similar to that of bone, PLA is non-toxic, has been approved by the US Food and Drug Administration (FDA), and possesses a high mechanical strength [52–54]. However, PLA exhibits insufficient mechanical strength for load bearing and a lack of cell affinity because of its hydrophobic surface characteristics, resulting in insufficient interaction with the bone tissue [53,55,56]. Moreover, PLA decreases the pH of the body fluids, whereas degradation occurs within the physiological environment, which can cause inflammatory reactions [53,57].

Magnesium (Mg), which is a biodegradable metal, is an essential element in the human body that plays an important role in human metabolism [58–60]. Mg has good bioactivity via the release of Mg^{2+} ions during its degradation, resulting in the acceleration of bone growth; therefore, it induces a better fixation of the implant to the surrounding bone tissue [61,62]. In addition, Mg has a high mechanical strength and an elastic modulus similar to that of bone compared with the other biometals [58–60] that are applied as composite reinforcers to improve the mechanical performance of the polymer matrix [55,58,63]. Mg has been used to reinforce PLA in low contents up to 7 wt% [63] or 15 wt% [55] which was limited by difficulty in uniform of high contents of Mg in PLA matrix. Moreover, Mg has an inherent antibacterial property because of the release of Mg^{2+} ions and the increase in the pH, which can effectively inhibit bacterial infection [64]. Furthermore, Mg presents the characteristics of absorbing laser light and generating heat, which can induce local hyperthermia, thus preventing bacterial infection. Thus, Mg is a good candidate as a reinforcer of the PLA matrix, to enhance its mechanical and biological performance and add a photothermal antibacterial property [65–68].

Herein, we fabricated an antibacterial PLA/Mg composite via a high-shear mixing process for the homogeneous dispersion of high contents of Mg (15 and 30 vol%) in the PLA matrix, to enhance the mechanical and biological performance of the matrix; this composite would be a great potential material for the fabrication of biodegradable orthopedic implants. The PLA/Mg composite exhibited improved compressive strength and stiffness together with a controlled degradation property. In addition, as shown in Fig. 1, the release of Mg^{2+} ions and the generation of a micro-roughness on the surface of the composite via the degradation of Mg enhanced the initial cell attachment and bioactivity of PLA, to promote bone growth. Furthermore, the PLA/Mg composite exhibited an antibacterial effect based on the inherent antibacterial property of Mg [64] and the generation of localized heat after the application of a NIR laser on the composite. Therefore, the antibacterial PLA/Mg composite fabricated here using a high-shear mixer may be a great candidate material for application in the fabrication of biodegradable orthopedic implants.

2. Experimental section

2.1. Fabrication of PLA/Mg composites

2.1.1. Material preparation

PLA pellets (Ingeo 4032D, Nature Works LLC, USA) and Mg powder (between 100 and 200 mesh, 99.6 %, Alfa Aesar, USA) were prepared to fabricate PLA/Mg composites. Mg powder was characterized by observing the morphology with scanning electron microscope (SEM, JSM 6360, JEOL, Japan) and confirming the chemical composition with X-ray diffraction (D8-Advance, BRUKER, Germany) with a Cu Kα source at a scan speed of 1°/min. Irregular shape with average size of ~120 μm Mg particles were used as reinforcers (Fig. S1). PLA/Mg composite was fabricated in three different methods including dissolving method, melting method, and high-shear mixing method as shown in Fig. S2.

2.1.2. Dissolving method

Dissolving method was performed by dissolving PLA in dichloromethane (DCM, Sigma Aldrich, USA) with 40 w/v% and mixing Mg powder by 30 vol% of the amount of PLA dissolved in DCM. The solution was dried at 70 °C for 24 h to eliminate DCM. Dried PLA/Mg mixture was hot pressed using the metal mold with 12 mm in diameter by hand press machine (hydraulic unit model 3925, Carver, USA) at 170 °C with 5000 N to fabricate cylindrical composite sample.

2.1.3. Melting method

Melting method was performed by melting PLA pellets at 180 °C in dry oven and mixing Mg powders in molten PLA. The molten PLA/Mg

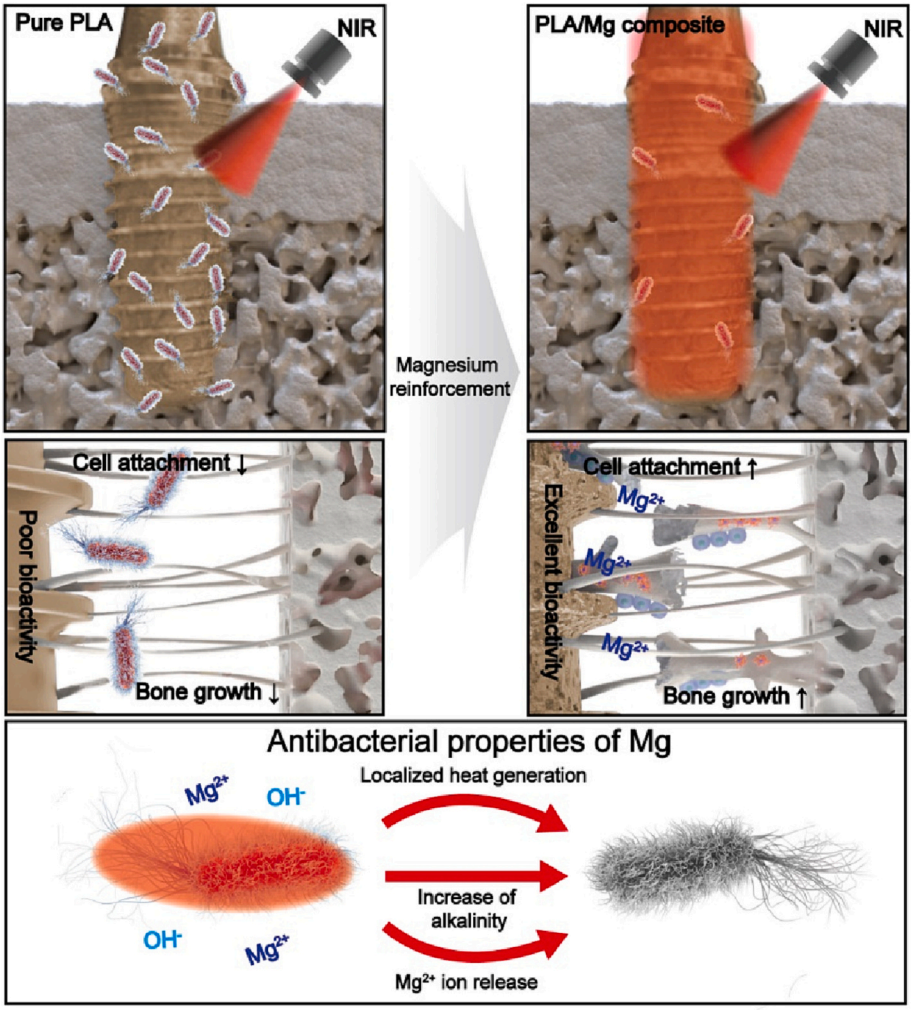

Fig. 1. Schematic representation of the antibacterial PLA/Mg composite for use in biodegradable orthopedic implants.

mixture was immersed inside the metal mold and hot pressed in equivalent conditions with those of dissolving method.

2.1.4. High-shear mixing method

Lastly, high-shear mixing method was performed by homogeneously mixing molten PLA with Mg powder using a high-shear mixer at 180 °C and formed cylindrical composite sample using the metal mold and hot pressed as the prior methods. For characterization and evaluating mechanical and biological performances of PLA/Mg composite regarding to the contents of Mg, PLA/Mg composites with 15, and 30 vol% of Mg particles were fabricated by high-shear mixing method.

2.2. Characterization

The microstructures of pure PLA and PLA/Mg composites with 15, and 30 vol% of Mg were analyzed by observing the cross-section of the specimens with scanning electron microscope (SEM, JSM 6360, JEOL, Japan). The cross-section of PLA and PLA/Mg composites were obtained by cutting the specimen with low-speed diamond saw (No. 11–1280 ISOMET, Buehler, USA), and the surface of the cross-section was polished using the abrasive SiC papers from 400 to 800 grit prior to the SEM imaging. To evaluate the uniformity of dispersion of Mg powder in PLA matrix we performed the quantitative analysis with the SEM images. We utilized ImageJ software [69] for the initial processing of our images. First, we removed the background with a radius setting of 25. This was followed by denoising the images via application of a Gaussian filter with a kernel size of one. Subsequently, the post-processed images were binarized, employing the Otsu algorithm as shown in Fig. S3. Next, we implemented the watershed algorithm to isolate the particles in the images. Following the particle isolation, we performed a particle analysis to extract the coordinates of the identified particles. Afterwards, we calculated the particle density by adding Gaussian distribution to each coordinates and multiplied with the particles area for the weighting and expressed particle density map and variance as shown in Fig. S3. In addition, the chemical structures of the PLA and PLA/Mg composites with 15 and 30 vol% were evaluated by Fourier transform infrared spectroscopy (FT-IR, VERTEX80v, BRUKER, USA).

2.3. Mechanical behavior

The mechanical behaviors of pure PLA and PLA/Mg composites with 5, 10, 15, and 30 vol% were evaluated by compression tests using an Instron 5582 system (Instron, Norwood, USA) with a cross-head speed of 1 mm/min. All specimens were processed into the size of $4 \times 4 \times 6$ mm^3. Three specimens of each conditions were examined.

2.4. Degradation behavior

The degradation behavior of the PLA and PLA/Mg composites evaluated by monitoring pH change of simulated body fluid (SBF) and examining the change of compressive strength of the specimens. Specimens with the size of 12 mm in diameter and 12 mm length were

immersed in 20 ml of SBF (prepared by the method proposed by Kokubo et al. [70]) at 37 °C and the pH was measured by a pH meter (Orion 3 Star, Thermo Scientific, USA) at each time periods. Three specimens of each type were tested. Moreover, the Mg^{2+} ion release behavior was examined after immersion of PLA/Mg composites with a size of 12 mm in diameter and 1.5 mm length and by extracting SBF solution after predetermined time period. After extraction, specimens were transferred to fresh SBF solution. Mg^{2+} ion concentration of the extracted solution was measured with inductively coupled plasma atomic emission spectroscopy (ICP-AES, OPTIMA 8300, PerkinElmer, USA). Three specimens of each specimen conditions were tested. In addition, PLA and PLA/Mg composites with the size of 4 × 4 × 6 mm^3 were immersed in SBF and specimens were taken out at each time periods and measured the compressive strength by compression tests with a cross-head speed of 1 mm/min. Three specimens of each conditions were examined. Furthermore, surface morphologies PLA and PLA/Mg composites after degradation in SBF were observed. The specimens were immersed in SBF for 5 days and were taken out. The specimens were washed with deionized water (DI water) and dried before SEM observation. Surface morphologies were observed with SEM (S-4800, HITACHI, Japan).

2.5. In-vitro biological evaluation

2.5.1. In-vitro cell test preparation

In-vitro biological behavior of pure PLA and PLA/Mg composites was evaluated with pre-osteoblast cell (MC3T3-E1, ATCC, CRL-2593, USA). Prior to in-vitro cell test, specimens were cleansed in 70 % ethanol and further sterilized by UV radiation for 30 min. The cells were cultured in an alpha minimum essential medium (α-MEM, Welgene Biotech Co., Ltd., Korea) supplemented with 10 % fetal bovine serum (FBS; Gibco, USA) and 1 % antibiotic antimycotic solution (AA; Sigma-Aldrich, USA) in a humid incubator with 5 % CO_2 at 37 °C similar to previous article [71].

2.5.2. Initial cell attachment

Morphology of attached cells was observed with SEM and inverted fluorescence microscope (ECLIPS Ti2; Nikon, Japan) after 1 day of cell seeding with the density of 3 × 10^4 cells ml^{-1} on pure PLA, PLA/15Mg and PLA/30Mg with the size of 12 mm in diameter and 1.5 mm in height. The specimens for SEM observation were prepared by immersing the specimen in 2.5 % glutaraldehyde (Sigma Aldrich, USA) for 10 min, dehydrating in graded ethanol (70 %, 90 %, 95 %, and 100 % ethanol in sequence) and finally immersing in 1,1,1,3,3,3-hexamethyldisilazane (Sigma-Aldrich, USA) for 10 min. The specimens for fluorescent imaging were prepared by immersing the specimen in 4 % paraformaldehyde solution for 10 min and washed twice with Dulbecco's phosphate buffered saline (DPBS; Welgene Biotech Co., Ltd., Korea). The cells were permeabilized with 0.1 % Triton X-100 (Sigma-Aldrich, USA) diluted with DPBS for 5 min and then washed with DPBS two times. In order to block the nonspecific site, we used 1 % bovine serum albumin (BSA; Sigma-Aldrich, USA), followed by staining of the F-actin and nuclei of the cells with phalloidin (Alexa Fluor® 555 phalloidin, Molecular Probes, USA) and 4′,5-diamidino-2-phenylindole (DAPI; ProLong Gold® antifade reagent with DAPI, Invitrogen, USA), respectively. Furthermore, cell coverage (%) and amounts of cells per unit area (mm^{-1}) were evaluated by measuring the area of cells occupying the surface of the specimens and counting the number of cell nucleus, respectively, with fluorescent image data using ImageJ software. Four images of each conditions were analyzed to evaluate the cell coverage and amounts of cells per unit area.

2.5.3. Cell proliferation

Cell proliferation was evaluated by measuring the DNA amount of the cells cultured on the specimens with the size of 12 mm in diameter and 1.5 mm in height using a Cyquant cell proliferation assay kit (C7026, Invitrogen, Carlsbad, CA) after 3 and 5 days of seeding with the density of 2 × 10^3 cells ml^{-1}. After the predetermined culturing periods, the cells adhered on every exposed area of the sample were detached by treating 1 ml of trypsin-EDTA for 4 min. Subsequently, 1 ml of culturing medium was supplemented to neutralize trypsin-EDTA and cells were collected by centrifugation and removal of supernatant solution. Collected cells were treated using a 200 μl of fluorescent working solution and the DNA amount of cells was evaluated using a hybrid multimode reader (Synergy H1, BioTek, USA). The excitation and emission wavelength during the measurement were 480 and 535 nm, respectively. Three specimens of each conditions were tested.

2.5.4. Cell differentiation

Degree of differentiation was also assessed by alkaline phosphate (ALP) assay. MC3T3-E1 cells with concentration of 5 × 10^3 cells ml^{-1} were cultured on PLA, PLA/15Mg, and PLA/30Mg scaffolds with 12 mm in diameter and 1.5 mm in height. After 1 day of culturing, medium was changed by medium containing 10 mM of β-GP and 50 mg/ml of ascorbic acid. And the medium was refreshed every 3 days. At 7 days and 14 days of culturing, attached cells were detached by trypsin-EDTA for 4 min and collected through centrifugation at 1500 rpm for 5 min. Subsequently, collected cells were treated using 0.1 % Triton X-100 and additionally centrifuged 14,000 rpm for 20 min at 4 °C. ALP activity was assessed by measuring absorbance at 405 nm utilizing a multiple plate reader (Victor3, Perkin Elmer, Germany). Three specimens for each conditions were used for the ALP activity evaluation.

2.6. NIR-induced thermal evaluation

Photothermal ability of pure PLA and PLA/Mg composites was evaluated by applying 808-nm NIR laser (OCLA; AMI, Korea). Prior to laser irradiation, 60 μl of DI water was loaded onto the prepared specimens with the size of 8 × 8 × 1.5 mm^3 to mimic wet condition. NIR radiation was applied with different power (200, 400, and 600 mW) and the thermal images acquired and temperature was measured using the thermal imaging camera (FLIR E54; FLIR Systems Inc., USA).

2.7. Antibacterial effect evaluation

Antibacterial property of the pure PLA and PLA/Mg composites were determined by colony counting method using gram-negative *Escherichia coli* (*E. coli*; ATCC 8739, Rockville, MD, USA) and gram-positive *Staphylococcus aureus* (*S. aureus*; ATCC 6538, Rockville, MD, USA). Both of bacteria were cultured for 18 h by inoculation 50 μl of stock solution into 3 ml of Luria–Bertani (LB) broth (BD Difco™, USA). Specimens with the size of 8 × 8 × 1.5 mm^3 were sterilized using 70 % ethanol and 30 min of UV radiation. Subsequently, the specimens were fixed in the culture plate and subsequently 60 μl of prepared bacteria solution (1 × 10^8 CFU ml^{-1} for *E. coli* and 1 × 10^4 CFU ml^{-1} for *S. aureus*) was poured onto the specimens. After NIR radiation for 2 min with 400 mW of power, bacteria were cultured in a shaking incubator (SI-300R, Lab Companion, USA) at 200 rpm and 37 °C for 3 h. Succeedingly, attached live bacteria were detached from the specimen by vortex for 1 min in 3 ml of LB-broth. Obtained bacteria solution was diluted by 1/100 and 100 μl of the solution was spread on agar plate (LB agar, BD Difco™, USA) and incubated in humidified oven at 37 °C for 24 h. The average colony numbers of each *E. coli* and *S. aureus* were counted based on optical images taken by digital camera. Three specimens of each conditions were evaluated.

2.8. Statistical analysis

All quantitative data were statistically analyzed using IBM SPSS Statistics 26 (IBM, Armonk, NY, USA), and the data were expressed as the mean ± standard deviation. The statistical analysis was performed by a one-way analysis of variance with Tukey's post hoc comparison. The data were denoted with the following symbols, respectively: (*) for *p*-

values (probability) <0.05 ($p < 0.05$), (**) for $p < 0.01$, (***) for $p < 0.005$, and (****) for $p < 0.001$.

3. Results and discussion

3.1. Characterization

We assessed the surface and cross-sectional morphologies of PLA/Mg composites with 30 vol% of Mg according to the fabrication methods, including the dissolution method, melting method, and high-shear mixing method (Fig. S2). Large pores were observed on the surface and inner cross-section of the PLA/Mg composite fabricated using the dissolving method (Fig. S3A and D). The pores were generated by the evaporation of the residual DCM solvent during the hot pressing procedure [72]. In turn, the PLA/Mg composites fabricated using the melting method and high-shear mixing method exhibited a dense structure without any pores or defects on the surface and inner structure of the specimens. In addition, the compressive strength of the pure PLA and PLA/Mg composites was examined, to assess the mechanical performance of PLA/Mg composites according to the fabrication method, as shown in Fig. S4. The pure PLA material exhibited an average compressive strength of 68.8 MPa, whereas the average compressive strength of the PLA/Mg composite fabricated using the dissolution method decreased to 56.8 MPa, as shown in Fig. S4, because of the formation of pores formed inside the composite [73,74]. In contrast, the compressive strength of the PLA/Mg composite fabricated using the melting method and the high-shear mixing method was enhanced up to 90.1 and 93.2 MPa, respectively; this reinforcement was afforded by the Mg particles inside the PLA matrix [75]. Although the PLA/Mg composites fabricated using these two methods had a dense structure with enhanced mechanical strength, the composite that was fabricated using the melting method exhibited a non-uniform distribution of Mg particles inside the PLA matrix, which was caused by the agglomeration of Mg particles during the mixing of the molten PLA and Mg particles manually (Fig. S3). In turn, the Mg/PLA composite with 30 vol% of Mg fabricated using the high-shear mixing method had a dense structure with homogenous dispersion of Mg particles (Fig. S3). To confirm uniform dispersion of Mg powder in PLA matrix by high-shear mixing method, particle density map and variance was calculated as shown in Fig. S3. PLA/Mg composite fabricated by high-shear mixing method had less color density gradient and lower variance value which verify better uniformity of Mg dispersion. In addition, PLA/Mg composite fabricated by high-shear mixing method exhibited an enhanced mechanical strength (Fig. S4), which indicated that this method is suitable to fabricate PLA/Mg composites with a high content of the Mg reinforcer. As a result, PLA/Mg composites with 15 and 30 vol% of Mg were fabricated using the high-shear mixing method for further examinations, and were termed as PLA/15Mg and PLA/30Mg, respectively.

Pure PLA, PLA/15Mg, and PLA/30Mg were fabricated in a dense cylindrical structure via the high-shear mixing method (Fig. 2A–C). We examined the cross-sectional morphologies of the pure PLA and PLA/Mg composites. Mg particles (shown in bright contrast) were homogeneously dispersed inside the PLA matrix, and defects or pores were not observed inside the composites (Fig. 2D–F), which indicates that the high-shear mixing method should be the preferred method to fabricate PLA/Mg composites with a high content of Mg particles. Furthermore, chemical structure of PLA/Mg composites was evaluated with FT-IR spectroscopy (Fig. S5). Pure PLA exhibited peaks related to stretching frequencies for -CH_3 asymmetric, -CH_3 symmetric, C═O, and C—O at 2997, 2947, 1746, and 1080 cm^{-1}, respectively, and bending frequencies for CH_3 asymmetric and -CH_3 symmetric, at 1450 and 1361 cm^{-1}, respectively, which are representative peaks of PLA [76]. PLA/Mg composite showed similar peaks to those of pure PLA, confirming no significant deterioration of chemical structure of PLA and PLA/Mg composites during heating and Mg incorporation procedures.

3.2. Mechanical behavior

We performed a compressive test to confirm the mechanical behaviors of the pure PLA and PLA/Mg composites. The compressive-

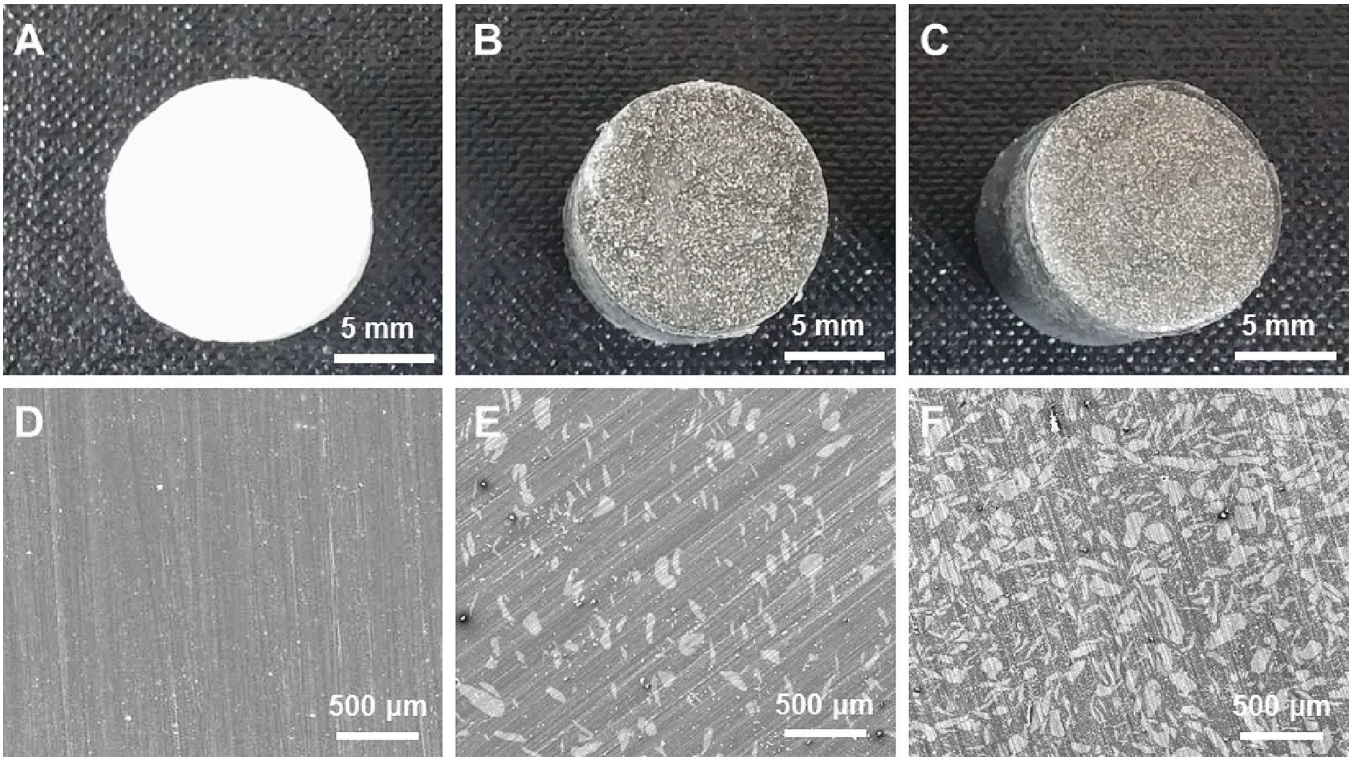

Fig. 2. Morphologies of the PLA/Mg composites. Optical microscopy (upper panel) and cross-sectional SEM (lower panel) images of (A, D) pure PLA, (B, E) PLA/15Mg, and (C, F) PLA/30Mg.

stress–strain curves of the pure PLA and PLA/Mg composites were examined, as shown Fig. 3A. The PLA/Mg composites exhibited a ductile behavior similar to that of pure PLA, despite the mixing of a high content of Mg accompanied by the heat treatment during the high-shear mixing and hot-pressing procedure, which may result in brittle PLA composites [77]. Pure PLA had an average compressive strength of 68.8 MPa, whereas PLA/15Mg and PLA/30Mg exhibited an enhanced compressive strength up to 107.3 and 93.2 MPa, respectively. The lower average compressive strength of PLA/30Mg compared with PLA/15Mg was attributed to the poor affinity of Mg to PLA, which has an adverse effect on the mechanical strength at high levels [55]. The stiffness of the pure PLA was measured as being 1.6 GPa, whereas stiffness of PLA/15Mg and PLA/30Mg increased up to 2.3 and 2.5 GPa, respectively. The increased stiffness of the Mg/PLA composite may accelerate osteogenesis, thus potentially providing a more appropriate micro-environment for osteoblasts [78]. In addition, mechanical behavior of PLA/Mg composites with lower amounts of Mg, 5 and 10 vol%, were examined to confirm the effect of Mg reinforcer (Fig. S5). Compressive strength and stiffness of PLA/5Mg and PLA/10Mg had a slight increase to 78.2 and 87.4 MPa, and 1.9 and 2.1 GPa, respectively compared with pure PLA, showing lower improvement compared with higher contents of Mg reinforcer (15 and 30 vol%).

3.3. Degradation behavior

The degradation behaviors of the pure PLA and PLA/Mg composites were evaluated by immersing each specimen in a simulated body fluid (SBF). At each time point, the pH of the solution was measured to analyze the pH variance of the SBF caused by the degradation of PLA and Mg (Fig. 4A). PLA showed almost no pH change, whereas in the PLA/Mg composites, the pH increased because of the degradation of Mg, which generated OH^- ions in the SBF [61,62,64]. The pH of the SBF increased rapidly up to 9.5 after 5 days of immersion of PLA/30Mg in the SBF, whereas PLA/15Mg immersion yielded a gradual increase in pH up to 8.5 after 5 days, because of the lower amount of Mg exposed at the PLA surface, as shown in Fig. 2E. Moreover, the concentration of Mg^{2+} ions which is one of the byproducts of Mg degradation was measured to evaluate the release behavior of Mg^{2+} ion (Fig. 4B). Similar with that of the pH variation, more amount of Mg was released from PLA/30Mg compared to the PLA/15Mg indicating that more amount of Mg were degrading from PLA/30Mg composites. In addition, the mechanical strength of the PLA/Mg composites was measured at each time point after the immersion of the specimens in the SBF as shown in Fig. 4C. PLA/30Mg showed a rapid decrease in compressive strength, to 67.2 MPa, after only 3 days of immersion, and decreased to 44.7 MPa (48 % decrease) after 5 days of immersion in the SBF because of the rapid degradation of Mg, which led to the formation of pores and defects [63]. In contrast, PLA/15Mg exhibited a gradual decrease in mechanical strength, to 78.0 MPa (27 % decrease), after 5 days, which indicated a great potential for application in biodegradable orthopedic implants. Furthermore, after 5 days of immersion in SBF, surface morphologies of PLA, PLA/15Mg, and PLA/30Mg were observed. There was no significant difference at the surface of PLA after 5 days of immersion in SBF, however, for PLA/Mg composites calcium phosphate (CaP) was observed on the surface of the composites which was formed by supersaturation during the increase in pH of SBF solution [79]. Moreover, microroughness formed on the surface of the composites with the degradation of Mg particles, which can enhance osseointegration [80]. However, PLA/30Mg showed cracks on the PLA surface which affected severe decrease in mechanical performances as shown in Fig. 4C.

3.4. In-vitro biological behavior

The initial cell-attachment morphologies of pre-osteoblast cells on pure PLA, PLA/15Mg, and PLA/30Mg were observed using SEM and an inverted fluorescence microscope after 1 day of cell culturing (Fig. 5A). All specimens exhibited a non-toxic behavior; however, lower amounts of cells were observed on PLA with a relatively linear morphology compared with the PLA/Mg composites. Higher amounts of cells with well-spread morphologies were observed on PLA/Mg composites, with cells tending to adhere near the Mg particles exposed on the surface of the PLA/Mg composites. In addition, the initial cell-attachment behavior of pure PLA and the PLA/Mg composites was evaluated quantitatively based on cell coverage (%) and cell count per unit area (mm^{-1}) using fluorescent images of the initial cell attachment. PLA/15Mg and PLA/30Mg exhibited a 1.98-fold and 1.66-fold increase in cell coverage, respectively, and a 1.74-fold and 1.53-fold increase in the amount of cells, respectively, compared with the pure PLA. The initial cell-attachment results indicated an enhanced bioactivity for the PLA/Mg composites compared with pure PLA, which was attributed to the release of Mg^{2+} ions as shown in Fig. 4B and the micro-roughness afforded by the PLA/Mg composites via the degradation of Mg particles on their surface as shown in Fig. 5A, thus affecting the attachment of pre-osteoblast cells [55,63].

The proliferation and differentiation of pre-osteoblast cells were evaluated using a DNA assay and ALP activity assay after culturing the cells on pure PLA and PLA/Mg composites for 3 and 5 days, and 7 and 14 days, respectively (Fig. 6). The PLA/15Mg composite exhibited a higher density of cells on the specimen compared with pure PLA. However, despite the good initial cell attachment onto PLA/30Mg, the amounts of attached cells were lower than those observed for the PLA/15Mg, and even lower than those of the pure PLA. In addition, PLA/15Mg exhibited a similar ALP activity to that of pure PLA after 7 and 14 days of cell culturing, whereas the ALP activity of PLA/30Mg was

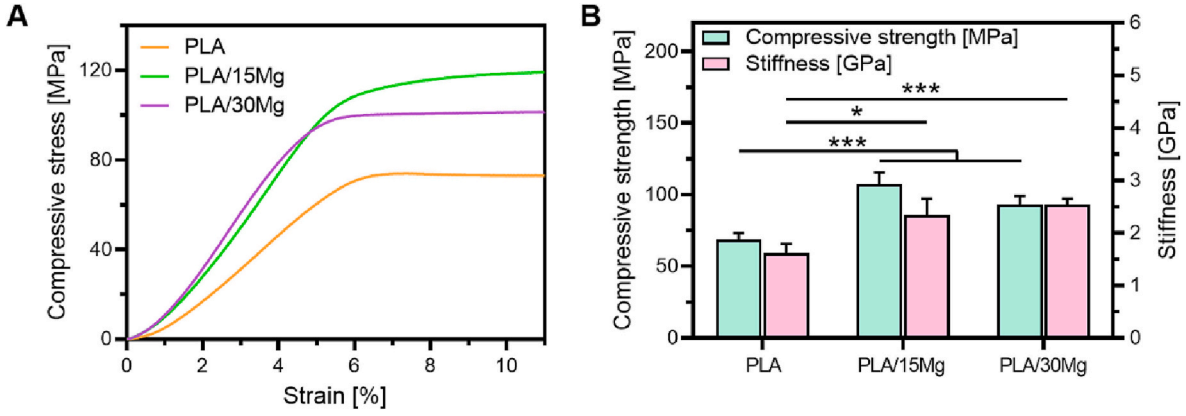

Fig. 3. Mechanical behavior of the PLA/Mg composites. (A) Compressive stress strain curve and (B) average compressive strength and stiffness of the PLA/Mg composites according to the volume ratio of Mg (*$p < 0.05$ and ***$p < 0.005$).

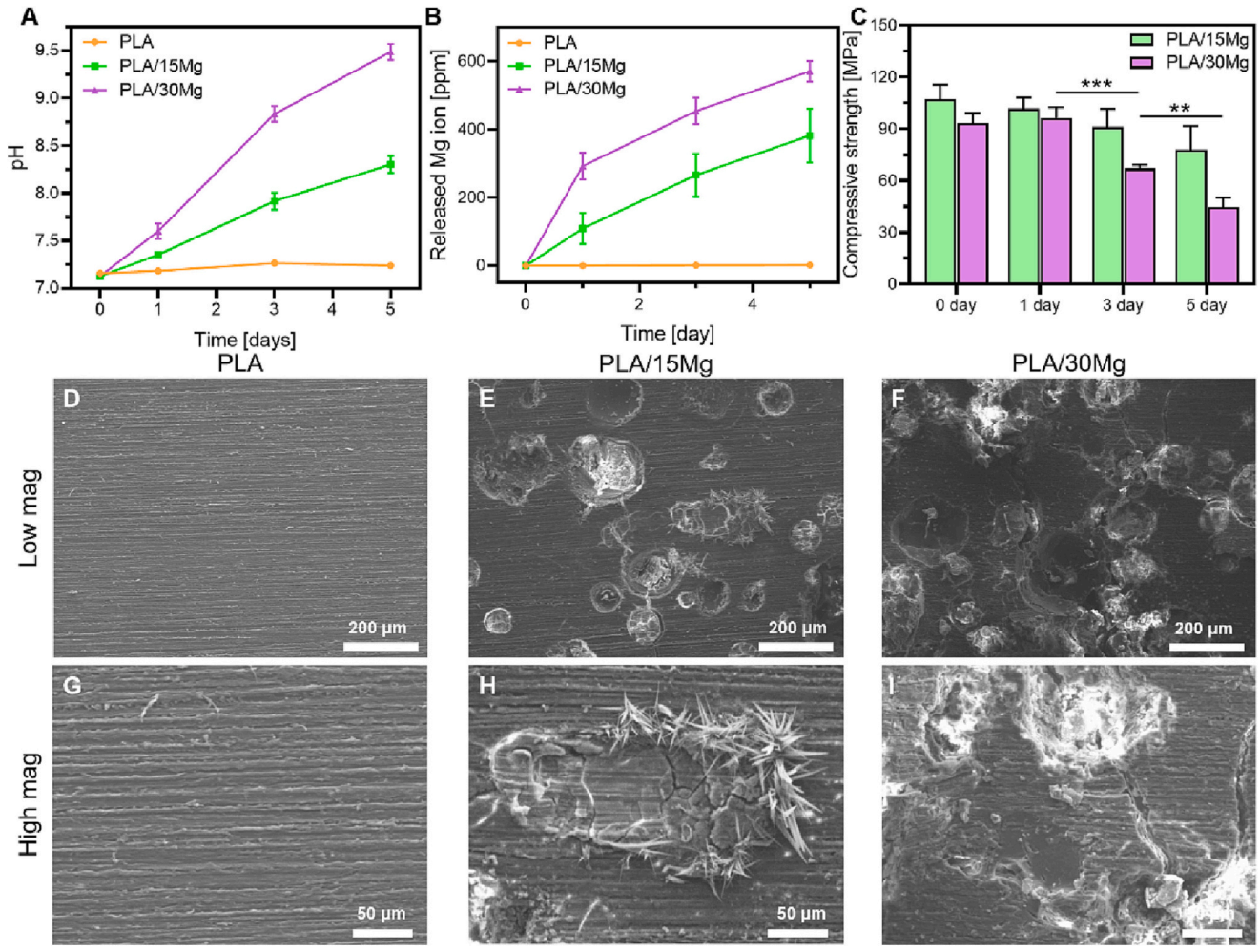

Fig. 4. Degradation behavior of the PLA/Mg composites. Variance of (A) the pH and (B) Mg^{2+} concentration of the SBF and (C) the average compressive strength of the PLA/Mg composites after the immersion of the specimens in the SBF (**$p < 0.01$ and ***$p < 0.005$). Surface morphologies of (D, G) PLA, (E, H) PLA/15Mg, and (F, I) PLA/30Mg after 5 days of immersion in SBF (upper panel: low magnification, bottom panel: high magnification).

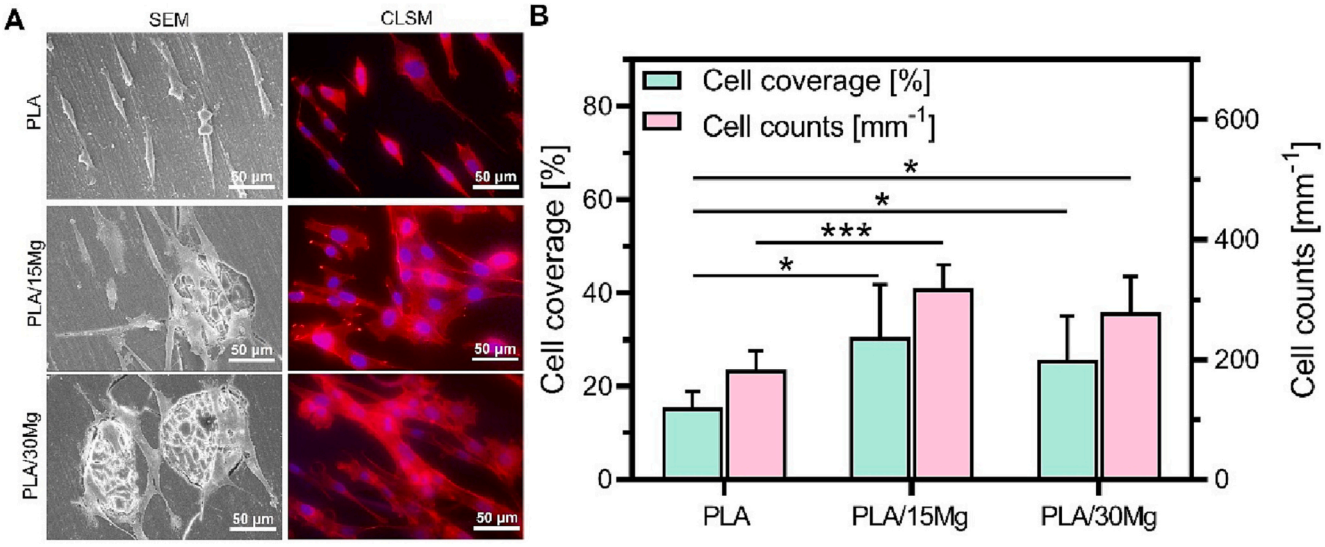

Fig. 5. Initial cell-attachment behavior of the PLA/Mg composites. (A) Representative SEM and fluorescence images of the initial cell-attachment morphology and (B) cell coverage and amounts of cells per unit area after 24 h of culturing pre-osteoblast cells (MC3T3-E1) on pure PLA and PLA/Mg composites (*$p < 0.05$, **$p < 0.01$, and ***$p < 0.005$).

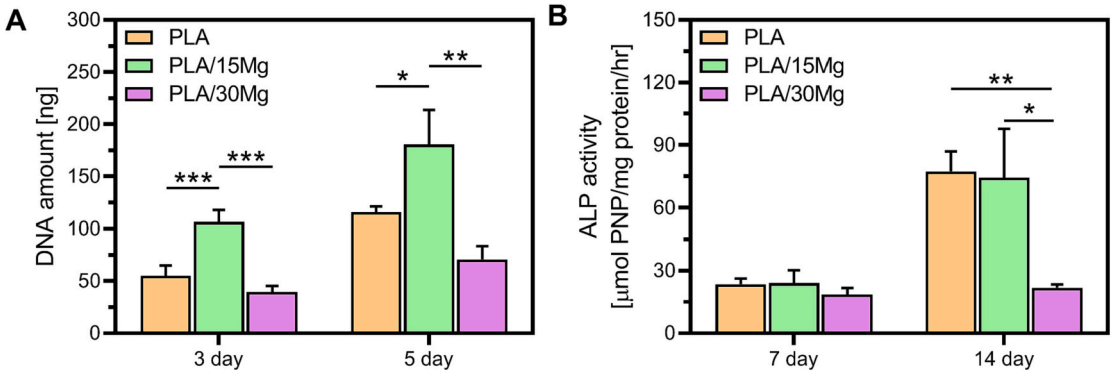

Fig. 6. Bioactivity of the PLA/Mg composites. (A) Cell proliferation and (B) ALP activity of MC3T3-E1 on pure PLA and PLA/Mg composites after culturing for 3 and 5 days, and 7 and 14 days, respectively (*$p < 0.05$, **$p < 0.01$, and, ***$p < 0.005$).

deteriorated after 14 days of culturing. Compared with the initial cell-attachment behavior, which was achieved in a short period, cell proliferation and differentiation exhibited a different tendency because of the change in the cell medium in the closed cell system during the long period of evaluation. PLA/15Mg showed a relatively mild environmental change, which afforded a cell-favorable effect that resulted in the preferred proliferation and differentiation of the pre-osteoblast cells. However, for PLA/30Mg, the rapid H_2 evolution and pH increase (Fig. 4A) during the long period of culturing in the closed cell system had an adverse effect on stable cell proliferation and differentiation [81,82].

3.5. Photothermal antibacterial activity

The idea of the "race to the surface" has been proposed to underscore the competition between bacterial cells and host cells for the surfaces of implanted biomaterials, because of the high risk of bacterial infection associated with implants [83]. The successful integration of implants into surrounding tissues is critical for preventing bacterial colonization and biofilm formation. Moreover, persistent infection after implantation may weaken the immune response and reduce the ability of neutrophils to destroy bacteria, resulting in immune evasion. Therefore, it is crucial to develop a preventive strategy to maintain an effective barrier against microorganisms after surgery. Using a photothermal therapy approach,

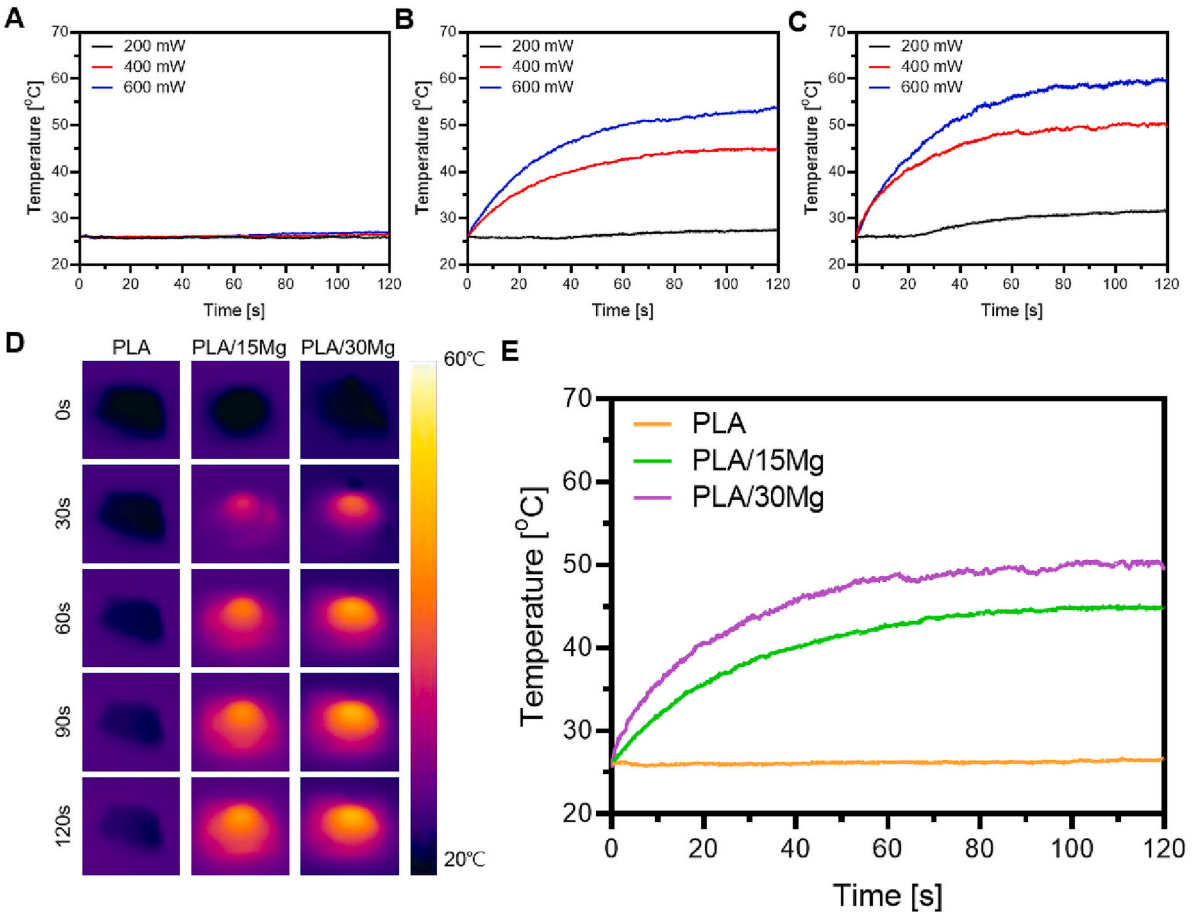

Fig. 7. Photothermal effect of the PLA/Mg composites. Monitoring of temperature elevation in (A) pure PLA, (B) PLA/15Mg, and (C) PLA/30Mg according to the power of the 808-nm NIR laser. (D) Thermal images and (E) temperature variance of the PLA/Mg composites after irradiation with a NIR laser at 400 mW.

we anticipate that PLA/Mg composites combined with NIR treatment will be able to inhibit bacterial colonization.

The photothermal effect of the pure PLA and PLA/Mg composites was evaluated by applying a near-infrared laser at 808 nm with different powers of 200, 400, and 800 mW (Fig. 7). The temperature of the pure PLA remained constant, regardless of the laser power, indicating a lack of photothermal effect for the pure PLA, as shown in Fig. 7A and D. In contrast, temperature of the PLA/15Mg and PLA/30Mg composites increased after the application of NIR irradiation, indicating a photothermal effect for these composites. In addition, as the power of the NIR laser increased, the temperature and rate of the temperature change increased, as shown in Fig. 7B and C. The photothermal effect is induced by the absorption of the laser light and its conversion to heat; however, the pure PLA does not have the ability to change the absorbed laser light to heat, which indicates the lack of heat generation by applying NIR irradiation [84,85]. In turn, Mg particles can transform the absorbed laser light into heat, which can increased the temperature by generating localized heat for the PLA/Mg composites [66]. We compared the photothermal effect of the specimens using a NIR laser at 400 mW. The temperature of PLA with 30 vol% of Mg increased faster and to a higher level (up to 50 °C) compared with PLA/15Mg, which increased up to 45 °C (Fig. 7E).

The antibacterial effects according to the Mg content and NIR application were analyzed using *Escherichia coli*, which are a representative Gram-negative bacterium, and *Staphylococcus aureus*, which is a representative Gram-positive bacterium (Fig. 8). The two bacteria were cultured in agar plates. The specimens were treated without or with the NIR laser. After the appropriate incubation time, the specimens were detached, optical images were captured (Fig. 8A and C), and the average colony number was counted (Fig. 8B and D). Fig. 8A and B shows the result obtained for *E. coli*, and Fig. 8C and D shows the results obtained for *S. aureus*. Before NIR treatment, PLA with Mg yielded fewer colonies of both bacteria because of the release of Mg^{2+} ions and the increase of the pH [64], which was reflected in the pH change observed during the Mg degradation (Fig. 4A). Furthermore, the application of the NIR laser at 400 mW generated localized heat for the PLA/Mg composites, as shown in Fig. 7D and E, resulting in a dramatic decrease in the number of colonies of the bacteria. NIR induces local heat generation from Mg particles which causes lysis of the bacterial membrane, and inactivation of essential proteins and enzymes of the bacteria [86–88]. This can avoid the concern of bacteria resistance and target the infected region which can minimize the adverse effect to surrounding tissues. Therefore, the PLA/Mg composites can prevent the initial infection via the inherent antibacterial effect of Mg, and can suppress the expansion of the infectious area via a photothermal effect after the implantation surgery, which is in alignment with recent studies for efficient antibacterial effects by applying multiple antibacterial pathways [89]. This indicates the potential of the PLA/Mg composite for antibacterial biodegradable orthopedic applications.

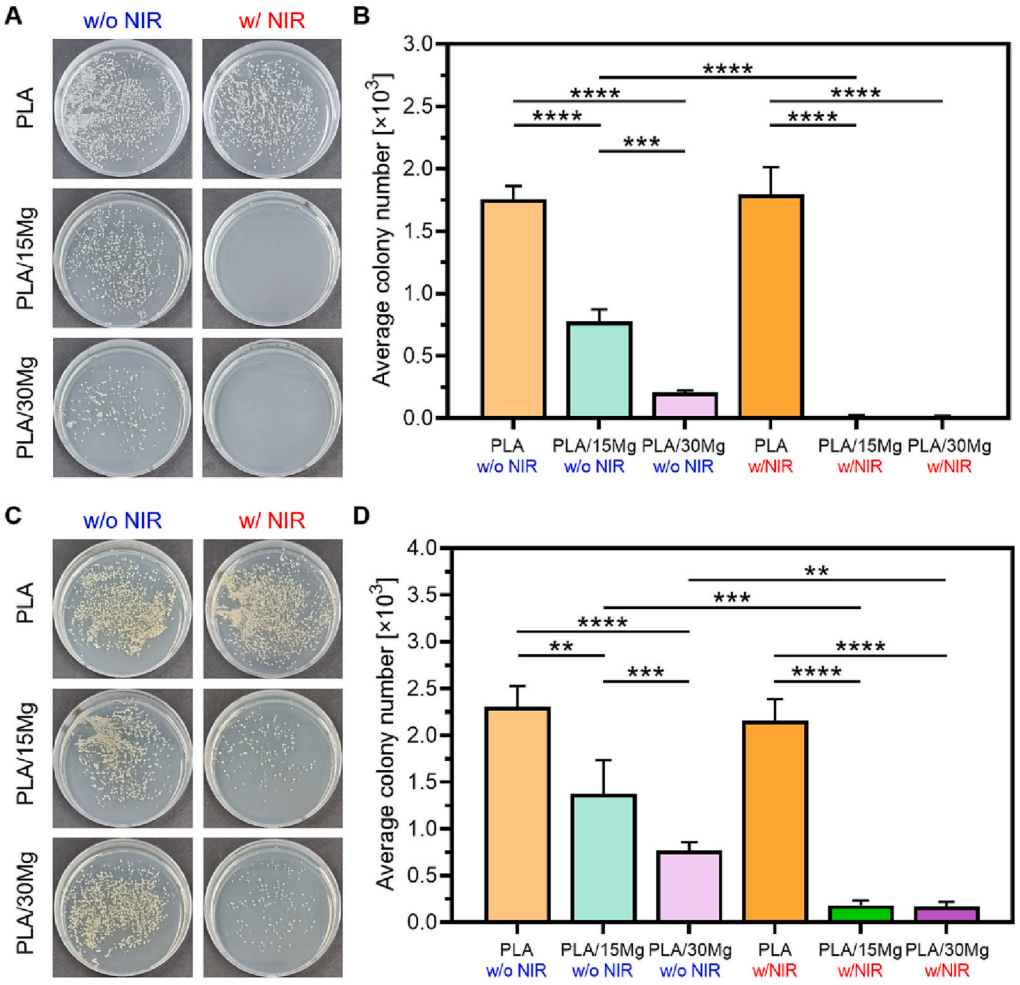

Fig. 8. Antibacterial effect of the PLA/Mg composites. (A) Optical images and (B) average colony number of *E. coli*; and (C) optical images and (D) average colony number of *S. aureus* cultured on agar plates after detachment from PLA/Mg composites with and without 808-nm NIR radiation (**$p < 0.01$, *** $p < 0.005$, and **** $p < 0.001$).

3.6. Antibacterial PLA/Mg composite for the production of biodegradable orthopedic implants

The PLA/Mg composite is a great candidate material for the production of biodegradable orthopedic implants, as it showed enhanced mechanical and biological performance with antibacterial properties compared with pure PLA—a commonly used biodegradable polymer. Mg particle mixed with PLA afforded an inherent antibacterial property by releasing Mg^{2+} ions and causing a high alkalinity, which is triggered by the release of OH^- ions during the degradation of Mg [64]. Moreover, the Mg particle is a photothermal agent that can generate localized heat via the application of near-infrared (NIR) irradiation, to prevent infection at the wound site after the implantation. In addition, Mg^{2+} ions are released during the degradation of Mg, and a micro-roughness and pores form on the surface of the PLA/Mg composite, which can improve cell attachment and accelerate bone growth on the surface of the implant. Consequently, the occurrence of Mg degradation in the composite improves the fixation of the implant to the surrounding bone tissues [63,90] compared with the pure PLA implant.

4. Conclusions

We fabricated an antibacterial Mg/PLA composite with homogeneous dispersion of Mg particles using the high-shear mixing method. The composite exhibited an enhanced mechanical and biological performance. Using homogeneously dispersed Mg as a reinforcer in the PLA matrix, the compressive strength and stiffness were enhanced; however, the mechanical strength deteriorated in the presence of an excessive amount of Mg (>30 vol%), because of the poor affinity between Mg and PLA. Moreover, the degradation rate of PLA/Mg could be controlled by adding Mg which has a faster degradation rate compared to PLA; in particular, PLA with 15 vol% of Mg showed a suitable degradation performance by exhibiting a gradual decrease in mechanical strength and gradual pH increase. This indicates the potential of the Mg/PLA composite for eliminating secondary surgery and maintaining the structure and strength of the material until the full healing of the surrounding tissue in orthopedic applications. In addition, the PLA/Mg composite with 15 vol% of Mg exhibited an improved biological performance, as indicated by the enhanced initial cell attachment and proliferation with moderate differentiation activity, which suggests the enhancement of the osteoconductivity and corresponding improved fixation to the surrounding bone tissue, for orthopedic applications. Furthermore, the PLA/Mg composite exhibited an antibacterial effect based on the inherent antibacterial property of Mg, which is mediated by the release of Mg^{2+} ions and the induction of an alkaline environment, together with the localized heat generated after NIR treatment; this may prevent infection after the surgery. The PLA/Mg composites exhibited a multi-functional performance based on their enhanced mechanical properties and bioactivity accompanied by a photothermal antibacterial effect. Therefore, the advanced PLA/Mg composite is a potential material for biodegradable orthopedic implants.

CRediT authorship contribution statement

Hyun Lee: Conceptualization, Methodology, Visualization, Investigation, Writing – original draft. **Da-Young Shin:** Conceptualization, Methodology, Visualization, Investigation. **Yuhyun Na:** Methodology, Investigation. **Ginam Han:** Methodology, Investigation. **Joodeok Kim:** Methodology, Software, Visualization. **Nahyun Kim:** Methodology, Visualization. **Seo-Jun Bang:** Methodology, Visualization. **Hyeong Seok Kang:** Methodology, Investigation. **SeKwon Oh:** Methodology, Validation. **Chang-Bun Yoon:** Methodology, Investigation. **Jungwon Park:** Methodology, Visualization. **Hyoun-Ee Kim:** Conceptualization, Methodology, Validation. **Hyun-Do Jung:** Conceptualization, Methodology, Validation, Data curation. **Min-Ho Kang:** Conceptualization, Methodology, Writing – review & editing, Supervision.

Declaration of competing interest

The authors declare that they have no known competing financial interests or personal relationships that could have appeared to influence the work reported in this paper.

Data availability

Data will be made available on request.

Acknowledgements

This work was supported by The Catholic University of Korea, Research Fund, 2022 and the National Research Foundation of Korea (NRF) grant funded by the Korea government (MSIT) (Nos. 2021R1I1A1A01043176, and 2021R1A2C1091301), the Technology Innovation program managed by the Ministry of Science and ICT, South Korea, the Ministry of Trade, Industry and Energy (MOTIE) (No. 20019192), Korean Fund for Regenerative Medicine (KFRM) grant funded by the Korea government (the Ministry of Science and ICT, the Ministry of Health & Welfare, KFRM 21A0501L1).

Appendix A. Supplementary data

Supplementary data to this article can be found online at https://doi.org/10.1016/j.bioadv.2023.213523.

References

[1] T.S. Jang, S.J. Park, J.E. Lee, J. Yang, S.H. Park, M.B.G. Jun, Y.W. Kim, C. Aranas, J.P. Choi, Y. Zou, Topography-supported nanoarchitectonics of hybrid scaffold for systematically modulated bone regeneration and remodeling, Adv. Funct. Mater. 32 (2022), 2206863, https://doi.org/10.1002/adfm.202206863.
[2] C. Stewart, B. Akhavan, S.G. Wise, M.M. Bilek, A review of biomimetic surface functionalization for bone-integrating orthopedic implants: mechanisms, current approaches, and future directions, Prog. Mater. Sci. 106 (2019), 100588, https://doi.org/10.1016/j.pmatsci.2019.100588.
[3] H. Lee, M.-K. Lee, G. Han, H.-E. Kim, J. Song, Y. Na, C.-B. Yoon, S. Oh, T.-S. Jang, H.-D. Jung, Customizable design of multiple-biomolecule delivery platform for enhanced osteogenic responses via 'tailored assembly system', Bio-Des. Manuf. 5 (2022) 451–464, https://doi.org/10.1007/s42242-022-00190-7.
[4] H. Lee, M.-K. Lee, K.-H. Cheon, I.-G. Kang, C. Park, T.-S. Jang, G. Han, H.-E. Kim, J. Song, H.-D. Jung, Functionally assembled metal platform as lego-like module system for enhanced mechanical tunability and biomolecules delivery, Mater. Des. 207 (2021), 109840, https://doi.org/10.1016/j.matdes.2021.109840.
[5] Z. Sheikh, S. Najeeb, Z. Khurshid, V. Verma, H. Rashid, M. Glogauer, Biodegradable materials for bone repair and tissue engineering applications, Materials 8 (2015) 5744–5794, https://doi.org/10.3390/ma8095273 (Basel).
[6] C.R. Arciola, D. Campoccia, L. Montanaro, Implant infections: adhesion, biofilm formation and immune evasion, Nat. Rev. Microbiol. 16 (2018) 397–409, https://doi.org/10.1038/s41579-018-0019-y.
[7] M. Wang, H. Li, Y. Yang, K. Yuan, F. Zhou, H. Liu, Q. Zhou, S. Yang, T. Tang, A 3D-bioprinted scaffold with doxycycline-controlled BMP2-expressing cells for inducing bone regeneration and inhibiting bacterial infection, Bioact. Mater. 6 (2021) 1318–1329, https://doi.org/10.1016/j.bioactmat.2020.10.022.
[8] M. Hosseini, N. Hassani Besheli, D. Deng, C. Lievens, Y. Zuo, S.C.G. Leeuwenburgh, F. Yang, Facile post modification synthesis of copper-doped mesoporous bioactive glass with high antibacterial performance to fight bone infection, Biomater. Adv. 144 (2023), 213198, https://doi.org/10.1016/j.bioadv.2022.213198.
[9] F. Pahlevanzadeh, R. Emadi, M. Setayeshmehr, M. Kharaziha, S.A. Poursamar, Antibacterial amorphous magnesium phosphate/graphene oxide for accelerating bone regeneration, Biomater. Adv. 138 (2022), 212856, https://doi.org/10.1016/j.bioadv.2022.212856.
[10] J. Josse, F. Velard, S.C. Gangloff, *Staphylococcus aureus* vs. osteoblast: relationship and consequences in osteomyelitis, Front. Cell. Infect. Microbiol. 5 (2015) 85, https://doi.org/10.3389/fcimb.2015.00085.
[11] J. Josse, F. Valour, Y. Maali, A. Diot, C. Batailler, T. Ferry, F. Laurent, Interaction between staphylococcal biofilm and bone: how does the presence of biofilm promote prosthesis loosening? Front. Microbiol. 10 (2019) 1602, https://doi.org/10.3389/fmicb.2019.01602.
[12] H. Wang, X. Xu, X. Wang, W. Qu, Y. Qing, S. Li, B. Chen, B. Ying, R. Li, Y. Qin, Performance optimization of biomimetic ant-nest silver nanoparticle coatings for antibacterial and osseointegration of implant surfaces, Biomater. Adv. 149 (2023), 213394, https://doi.org/10.1016/j.bioadv.2023.213394.
[13] M. Shimabukuro, K. Hayashi, R. Kishida, A. Tsuchiya, K. Ishikawa, Surface functionalization with copper endows carbonate apatite honeycomb scaffold with

antibacterial, proangiogenic, and pro-osteogenic activities, Biomater. Adv. 135 (2022), 212751, https://doi.org/10.1016/j.bioadv.2022.212751.
[14] Y. Cui, H. Liu, Y. Tian, Y. Fan, S. Li, G. Wang, Y. Wang, C. Peng, D. Wu, Dual-functional composite scaffolds for inhibiting infection and promoting bone regeneration, Mater. Today Bio 16 (2022), 100409, https://doi.org/10.1016/j.mtbio.2022.100409.
[15] S. Afewerki, N. Bassous, S. Harb, C. Palo-Nieto, G.U. Ruiz-Esparza, F.R. Marciano, T.J. Webster, A.S.A. Furtado, A.O. Lobo, Advances in dual functional antimicrobial and osteoinductive biomaterials for orthopaedic applications, Nanomed. Nanotechnol. Biol. Med. 24 (2020), 102143, https://doi.org/10.1016/j.nano.2019.102143.
[16] M. Ansari, Bone tissue regeneration: biology, strategies and interface studies, Prog. Biomater. 8 (2019) 223–237, https://doi.org/10.1007/s40204-019-00125-z.
[17] F. Pahlevanzadeh, M. Setayeshmehr, H.R. Bakhsheshi-Rad, R. Emadi, M. Kharaziha, S.A. Poursamar, A.F. Ismail, S. Sharif, X. Chen, F. Berto, A review on antibacterial biomaterials in biomedical applications: from materials perspective to bioinks design, Polymers 14 (2022) 2238, https://doi.org/10.3390/polym14112238.
[18] J. Aragón, S. Feoli, S. Irusta, G. Mendoza, Composite scaffold obtained by electro-hydrodynamic technique for infection prevention and treatment in bone repair, Int. J. Pharm. 557 (2019) 162–169, https://doi.org/10.1016/j.ijpharm.2018.12.002.
[19] C.T. Johnson, A.J. García, Scaffold-based anti-infection strategies in bone repair, Ann. Biomed. Eng. 43 (2015) 515–528, https://doi.org/10.1007/s10439-014-1205-3.
[20] C. Klein, M. Monet, V. Barbier, A. Vanlaeys, A.C. Masquelet, R. Gouron, R. Mentaverri, The Masquelet technique: current concepts, animal models, and perspectives, J. Tissue Eng. Regen. Med. 14 (2020) 1349–1359, https://doi.org/10.1002/term.3097.
[21] K. Amin, W.S. Khor, A. Rosich-Medina, V. Beale, Alveolar bone grafting: donor site review of 100 consecutive cases in cleft lip and palate, Cleft Palate Craniofac. J. 54 (2017) 137–141, https://doi.org/10.1597/15-180.
[22] E. Chiarello, M. Cadossi, G. Tedesco, P. Capra, C. Calamelli, A. Shehu, S. Giannini, Autograft, allograft and bone substitutes in reconstructive orthopedic surgery, Aging Clin. Exp. Res. 25 (2013) 101–103, https://doi.org/10.1007/s40520-013-0088-8.
[23] M. Catagni, W. Azzam, F. Guerreschi, L. Lovisetti, P. Poli, M. Khan, L. Di Giacomo, Trifocal versus bifocal bone transport in treatment of long segmental tibial bone defects: a retrospective comparative study, Bone Joint J. 101 (2019) 162–169, https://doi.org/10.1302/0301-620X.101B2.BJJ-2018-0340.R2.
[24] S. Zhang, H. Wang, J. Zhao, P. Xu, H. Shi, W. Mu, Treatment of post-traumatic chronic osteomyelitis of lower limbs by bone transport technique using mono-lateral external fixator: follow-up study of 18 cases, J. Orthop. Sci. 21 (2016) 493–499, https://doi.org/10.1016/j.jos.2016.04.010.
[25] S.S. Evans, E.A. Repasky, D.T. Fisher, Fever and the thermal regulation of immunity: the immune system feels the heat, Nat. Rev. Immunol. 15 (2015) 335–349, https://doi.org/10.1038/nri3843.
[26] Y. Wu, Q. Liao, L. Wu, Y. Luo, W. Zhang, M. Guan, H. Pan, L. Tong, P.K. Chu, H. Wang, ZnL2-BPs integrated bone scaffold under sequential photothermal mediation: a win–win strategy delivering antibacterial therapy and fostering osteogenesis thereafter, ACS Nano 15 (2021) 17854–17869, https://doi.org/10.1021/acsnano.1c06062.
[27] S.H. Kim, E.B. Kang, C.J. Jeong, S.M. Sharker, I. In, S.Y. Park, Light controllable surface coating for effective photothermal killing of bacteria, ACS Appl. Mater. Interfaces 7 (2015) 15600–15606, https://doi.org/10.1021/acsami.5b04321.
[28] K. Saravanakumar, A. Sathiyaseelan, P. Manivasagan, M.S. Jeong, M. Choi, E.-S. Jang, V.V. Priya, M.-H. Wang, Photothermally responsive chitosan-coated iron oxide nanoparticles for enhanced eradication of bacterial biofilms, Biomater. Adv. 141 (2022), 213129, https://doi.org/10.1016/j.bioadv.2022.213129.
[29] H. Tian, J. Hong, C. Li, Y. Qiu, M. Li, Z. Qin, R.A. Ghiladi, X. Yin, Electrospinning membranes with Au@carbon dots: low toxicity and efficient antibacterial photothermal therapy, Biomater. Adv. 142 (2022), 213155, https://doi.org/10.1016/j.bioadv.2022.213155.
[30] C. Wang, H. Tao, L. Cheng, Z. Liu, Near-infrared light induced in vivo photodynamic therapy of cancer based on upconversion nanoparticles, Biomaterials 32 (2011) 6145–6154, https://doi.org/10.1016/j.biomaterials.2011.05.007.
[31] L. Zhang, G. Oudeng, F. Wen, G. Liao, Recent advances in near-infrared-II hollow nanoplatforms for photothermal-based cancer treatment, Biomater. Res. 26 (2022) 1–28, https://doi.org/10.1186/s40824-022-00308-z.
[32] M.A. Kim, C.-M. Lee, NIR-mediated drug release and tumor theranostics using melanin-loaded liposomes, Biomater. Res. 26 (2022) 22, https://doi.org/10.1186/s40824-022-00270-w.
[33] L. Zhan, X. Yin, Y. Zhang, J. Ju, Y. Wu, L. Ding, C. Li, X. Chen, Y. Wang, Polydopamine-guarded metal-organic frameworks as co-delivery systems for starvation-assisted chemo-photothermal therapy, Biomater. Adv. 146 (2023), 213306, https://doi.org/10.1016/j.bioadv.2023.213306.
[34] Y. Zhao, X. Peng, D. Wang, H. Zhang, Q. Xin, M. Wu, X. Xu, F. Sun, Z. Xing, L. Wang, Chloroplast-inspired scaffold for infected bone defect therapy: towards stable photothermal properties and self-defensive functionality, Adv. Sci. 9 (2022), 2204535, https://doi.org/10.1002/advs.202204535.
[35] R. Nie, Y. Sun, H. Lv, M. Lu, H. Huangfu, Y. Li, Y. Zhang, D. Wang, L. Wang, Y. Zhou, 3D printing of MXene composite hydrogel scaffolds for photothermal antibacterial activity and bone regeneration in infected bone defect models, Nanoscale 14 (2022) 8112–8129, https://doi.org/10.1039/D2NR02176E.
[37] F. Matassi, A. Botti, L. Sirleo, C. Carulli, M. Innocenti, Porous metal for orthopedics implants, Clin. Cases Miner. Bone Metab. 10 (2013) 111–115.
[38] K.-H. Cheon, C. Park, M.-H. Kang, I.-G. Kang, M.-K. Lee, H. Lee, H.-E. Kim, H.-D. Jung, T.-S. Jang, Construction of tantalum/poly (ether imide) coatings on magnesium implants with both corrosion protection and osseointegration properties, Bioact. Mater. 6 (2021) 1189–1200, https://doi.org/10.1016/j.bioactmat.2020.10.007.
[39] H.-D. Jung, Titanium And Its Alloys for Biomedical Applications, Multidisciplinary Digital Publishing Institute, 2021.
[40] L. Shi, L. Shi, L. Wang, Y. Duan, W. Lei, Z. Wang, J. Li, X. Fan, X. Li, S. Li, Z. Guo, The improved biological performance of a novel low elastic modulus implant, PLoS One 8 (2013), e55015, https://doi.org/10.1371/journal.pone.0055015.
[41] H. Asgharzadeh Shirazi, M.R. Ayatollahi, A. Asnafi, To reduce the maximum stress and the stress shielding effect around a dental implant-bone interface using radial functionally graded biomaterials, Comput. Methods Biomech. Biomed. Eng. 20 (2017) 750–759, https://doi.org/10.1080/10255842.2017.1299142.
[42] H. Lee, H.-D. Jung, M.-H. Kang, J. Song, H.-E. Kim, T.-S. Jang, Effect of HF/HNO3-treatment on the porous structure and cell penetrability of titanium (Ti) scaffold, Mater. Des. 145 (2018) 65–73, https://doi.org/10.1016/j.matdes.2018.02.059.
[43] H. Lee, T.-S. Jang, J. Song, H.-E. Kim, H.-D. Jung, Multi-scale porous Ti6Al4V scaffolds with enhanced strength and biocompatibility formed via dynamic freeze-casting coupled with micro-arc oxidation, Mater. Lett. 185 (2016) 21–24, https://doi.org/10.1016/j.matlet.2016.08.075.
[44] H.-D. Jung, H. Lee, H.-E. Kim, Y.-H. Koh, J. Song, Fabrication of mechanically tunable and bioactive metal scaffolds for biomedical applications, J. Vis. Exp. (2015), https://doi.org/10.3791/53279.
[45] O. Bostman, H. Pihlajamaki, Clinical biocompatibility of biodegradable orthopaedic implants for internal fixation: a review, Biomaterials 21 (2000) 2615–2621, https://doi.org/10.1016/S0142-9612(00)00129-0.
[46] J. Kulkova, N. Moritz, E.O. Suokas, N. Strandberg, K.A. Leino, T.T. Laitio, H.T. Aro, Osteointegration of PLGA implants with nanostructured or microsized beta-TCP particles in a minipig model, J. Mech. Behav. Biomed. Mater. 40 (2014) 190–200, https://doi.org/10.1016/j.jmbbm.2014.08.028.
[47] A.R. Amini, J.S. Wallace, S.P. Nukavarapu, Short-term and long-term effects of orthopedic biodegradable implants, J. Long-Term Eff. Med. Implants 21 (2011) 93–122, https://doi.org/10.1615/jlongtermeffmedimplants.v21.i2.10.
[48] X. Liu, J.M. Holzwarth, P.X. Ma, Functionalized synthetic biodegradable polymer scaffolds for tissue engineering, Macromol. Biosci. 12 (2012) 911–919, https://doi.org/10.1002/mabi.201100466.
[49] H. Tian, Z. Tang, X. Zhuang, X. Chen, X. Jing, Biodegradable synthetic polymers: preparation, functionalization and biomedical application, Prog. Polym. Sci. 37 (2012) 237–280, https://doi.org/10.1016/j.progpolymsci.2011.06.004.
[50] J.-H. Ahn, J. Kim, G. Han, D. Kim, K.-H. Cheon, H. Lee, H.-E. Kim, Y.-J. Kim, T.-S. Jang, H.-D. Jung, 3D-printed biodegradable composite scaffolds with significantly enhanced mechanical properties via the combination of binder jetting and capillary rise infiltration process, Addit. Manuf. 41 (2021), 101988, https://doi.org/10.1016/j.addma.2021.101988.
[51] S.-M. Kim, I.-G. Kang, K.-H. Cheon, T.-S. Jang, H.-E. Kim, H.-D. Jung, M.-H. Kang, Enhanced bioactivity of micropatterned hydroxyapatite embedded poly (L-lactic) acid for a load-bearing implant, Polymers 12 (2020) 2390, https://doi.org/10.3390/polym12102390.
[52] S. Farah, D.G. Anderson, R. Langer, Physical and mechanical properties of PLA, and their functions in widespread applications—a comprehensive review, Adv. Drug Deliv. Rev. 107 (2016) 367–392, https://doi.org/10.1016/j.addr.2016.06.012.
[53] S. Tajbakhsh, F. Hajiali, A comprehensive study on the fabrication and properties of biocomposites of poly(lactic acid)/ceramics for bone tissue engineering, Mater. Sci. Eng. C 70 (2017) 897–912, https://doi.org/10.1016/j.msec.2016.09.008.
[54] J. Lee, H. Lee, K.-H. Cheon, C. Park, T.-S. Jang, H.-E. Kim, H.-D. Jung, Fabrication of poly (lactic acid)/Ti composite scaffolds with enhanced mechanical properties and biocompatibility via fused filament fabrication (FFF)–based 3D printing, Addit. Manuf. 30 (2019), 100883, https://doi.org/10.1016/j.addma.2019.100883.
[55] M. Ben Abdeljawad, X. Carette, C. Argentati, S. Martino, M.-F. Gonon, J. Odent, F. Morena, R. Mincheva, J.-M. Raquez, Molecules (2021), https://doi.org/10.3390/molecules26195944.
[56] C. Park, Y.-J. Seong, I.-G. Kang, E.-H. Song, H. Lee, J. Kim, H.-D. Jung, H.-E. Kim, T.-S. Jang, Enhanced osseointegration ability of poly (lactic acid) via tantalum sputtering-based plasma immersion ion implantation, ACS Appl. Mater. Interfaces 11 (2019) 10492–10504, https://doi.org/10.1021/acsami.8b21363.
[57] J.-Y. Bae, J.-E. Won, J.-S. Park, H.-H. Lee, H.-W. Kim, Improvement of surface bioactivity of poly(lactic acid) biopolymer by sandblasting with hydroxyapatite bioceramic, Mater. Lett. 65 (2011) 2951–2955, https://doi.org/10.1016/j.matlet.2011.06.023.
[58] X. Li, C.L. Chu, L. Liu, X.K. Liu, J. Bai, C. Guo, F. Xue, P.H. Lin, P.K. Chu, Biodegradable poly-lactic acid based-composite reinforced unidirectionally with high-strength magnesium alloy wires, Biomaterials 49 (2015) 135–144, https://doi.org/10.1016/j.biomaterials.2015.01.060.
[59] H.R. Bakhsheshi-Rad, A.F. Ismail, M. Aziz, M. Akbari, Z. Hadisi, S.M. Khoshnava, E. Pagan, X. Chen, Co-incorporation of graphene oxide/silver nanoparticle into poly-L-lactic acid fibrous: a route toward the development of cytocompatible and antibacterial coating layer on magnesium implants, Mater. Sci. Eng. C 111 (2020), 110812, https://doi.org/10.1016/j.msec.2020.110812.
[60] H.R. Bakhsheshi-Rad, M. Akbari, A.F. Ismail, M. Aziz, Z. Hadisi, E. Pagan, M. Daroonparvar, X. Chen, Coating biodegradable magnesium alloys with electrospun poly-L-lactic acid-åkermanite-doxycycline nanofibers for enhanced biocompatibility, antibacterial activity, and corrosion resistance, Surf. Coat. Technol. 377 (2019), 124898, https://doi.org/10.1016/j.surfcoat.2019.124898.
[61] M.H. Kang, H. Lee, T.S. Jang, Y.J. Seong, H.E. Kim, Y.H. Koh, J. Song, H.D. Jung, Biomimetic porous Mg with tunable mechanical properties and biodegradation

rates for bone regeneration, Acta Biomater. 84 (2019) 453–467, https://doi.org/10.1016/j.actbio.2018.11.045.
[62] M.H. Kang, T.S. Jang, H.D. Jung, S.M. Kim, H.E. Kim, Y.H. Koh, J. Song, Poly(ether imide)-silica hybrid coatings for tunable corrosion behavior and improved biocompatibility of magnesium implants, Biomed. Mater. 11 (2016), 035003, https://doi.org/10.1088/1748-6041/11/3/035003.
[63] P. Wan, C. Yuan, L. Tan, Q. Li, K. Yang, Fabrication and evaluation of bioresorbable PLLA/magnesium and PLLA/magnesium fluoride hybrid composites for orthopedic implants, Compos. Sci. Technol. 98 (2014) 36–43, https://doi.org/10.1016/j.compscitech.2014.04.011.
[64] Z. Lin, X. Sun, H. Yang, The role of antibacterial metallic elements in simultaneously improving the corrosion resistance and antibacterial activity of magnesium alloys, Mater. Des. 198 (2021), 109350, https://doi.org/10.1016/j.matdes.2020.109350.
[65] W. Zhou, Y. Zhang, S. Meng, C. Xing, M. Ma, Z. Liu, C. Yang, T. Kong, Micro-/nano-structures on biodegradable magnesium@PLGA and their cytotoxicity, photothermal, and anti-tumor effects, Small Methods 5 (2021), 2000920, https://doi.org/10.1002/smtd.202000920.
[66] Y. Zhang, C. Li, W. Zhang, J. Deng, Y. Nie, X. Du, L. Qin, Y. Lai, 3D-printed NIR-responsive shape memory polyurethane/magnesium scaffolds with tight-contact for robust bone regeneration, Bioact. Mater. 16 (2022) 218–231, https://doi.org/10.1016/j.bioactmat.2021.12.032.
[67] J. Long, W. Zhang, Y. Chen, B. Teng, B. Liu, H. Li, Z. Yao, D. Wang, L. Li, X.-F. Yu, L. Qin, Y. Lai, Multifunctional magnesium incorporated scaffolds by 3D-printing for comprehensive postsurgical management of osteosarcoma, Biomaterials 275 (2021), 120950, https://doi.org/10.1016/j.biomaterials.2021.120950.
[68] Z. Yuan, C. Lin, Y. He, B. Tao, M. Chen, J. Zhang, P. Liu, K. Cai, Near-infrared light-triggered nitric-oxide-enhanced photodynamic therapy and low-temperature photothermal therapy for biofilm elimination, ACS Nano 14 (2020) 3546–3562, https://doi.org/10.1021/acsnano.9b09871.
[69] J. Schindelin, I. Arganda-Carreras, E. Frise, V. Kaynig, M. Longair, T. Pietzsch, S. Preibisch, C. Rueden, S. Saalfeld, B. Schmid, J.-Y. Tinevez, D.J. White, V. Hartenstein, K. Eliceiri, P. Tomancak, A. Cardona, Fiji: an open-source platform for biological-image analysis, Nat. Methods 9 (2012) 676–682, https://doi.org/10.1038/nmeth.2019.
[70] T. Kokubo, H. Takadama, How useful is SBF in predicting in vivo bone bioactivity? Biomaterials 27 (2006) 2907–2915, https://doi.org/10.1016/j.biomaterials.2006.01.017.
[71] N. Kim, H. Lee, G. Han, M. Kang, S. Park, D.E. Kim, M. Lee, M.-J. Kim, Y. Na, S. Oh, S.-J. Bang, T.-S. Jang, H.-E. Kim, J. Park, S.R. Shin, H.-D. Jung, 3D-printed functional hydrogel by DNA-induced biomineralization for accelerated diabetic wound healing, Adv. Sci. (2023), 2300816, https://doi.org/10.1002/advs.202300816.
[72] N. Verdier, G. Foran, D. Lepage, A. Prebe, D. Ayme-Perrot, M. Dolle, Challenges in solvent-free methods for manufacturing electrodes and electrolytes for lithium-based batteries, Polymers 13 (2021), https://doi.org/10.3390/polym13030323 (Basel).
[73] D.-M. Liu, Influence of porosity and pore size on the compressive strength of porous hydroxyapatite ceramic, Ceram. Int. 23 (1997) 135–139, https://doi.org/10.1016/S0272-8842(96)00009-0.
[74] S.K. Kaliappan, A.A. Siyal, Z. Man, M. Lay, R. Shamsuddin, AIP Conf. Proc. (2018), 020066, https://doi.org/10.1063/1.5055468.
[75] I. Antoniac, L. Dragomir, I. Csaki, I. Mates, M. Vranceanu, Potential of the magnesium powder as filler for biomedical composites, Biomater. Tissue Technol. 1 (2017) 1–5, https://doi.org/10.15761/BTT.1000105.
[76] B.W. Chieng, N.A. Ibrahim, W.M.Z.W. Yunus, M.Z. Hussein, Poly(lactic acid)/poly(ethylene glycol) polymer nanocomposites: effects of graphene nanoplatelets, Polymers 6 (2014) 93–104, https://doi.org/10.3390/polym6010093.
[77] A. Nassar, M. Younis, M. Elzareef, E. Nassar, Effects of heat-treatment on tensile behavior and dimension stability of 3D printed carbon fiber reinforced composites, Polymers 13 (2021), https://doi.org/10.3390/polym13244305 (Basel).
[78] K. Chatterjee, S. Lin-Gibson, W.E. Wallace, S.H. Parekh, Y.J. Lee, M.T. Cicerone, M. F. Young, C.G. Simon Jr., The effect of 3D hydrogel scaffold modulus on osteoblast differentiation and mineralization revealed by combinatorial screening, Biomaterials 31 (2010) 5051–5062, https://doi.org/10.1016/j.biomaterials.2010.03.024.
[79] B.K. Sarma, B. Sarma, Journal of Physics: Conference Series, IOP Publishing, 2016, p. 012025, https://doi.org/10.1088/1742-6596/765/1/012025.
[80] R.A. Gittens, R. Olivares-Navarrete, Z. Schwartz, B.D. Boyan, Implant osseointegration and the role of microroughness and nanostructures: lessons for spine implants, Acta Biomater. 10 (2014) 3363–3371, https://doi.org/10.1016/j.actbio.2014.03.037.
[81] P. Saha, M. Roy, M.K. Datta, B. Lee, P.N. Kumta, Effects of grain refinement on the biocorrosion and in vitro bioactivity of magnesium, Mater. Sci. Eng. C 57 (2015) 294–303, https://doi.org/10.1016/j.msec.2015.07.033.
[82] S.M. Kim, J.H. Jo, S.M. Lee, M.H. Kang, H.E. Kim, Y. Estrin, J.H. Lee, J.W. Lee, Y. H. Koh, Hydroxyapatite-coated magnesium implants with improved in vitro and in vivo biocorrosion, biocompatibility, and bone response, J. Biomed. Mater. Res. A 102 (2014) 429–441, https://doi.org/10.1002/jbm.a.34718.
[83] R. Bright, D. Fernandes, J. Wood, D. Palms, A. Burzava, N. Ninan, T. Brown, D. Barker, K. Vasilev, Long-term antibacterial properties of a nanostructured titanium alloy surface: An in vitro study, Mater. Today Bio 13 (2022), 100176, https://doi.org/10.1016/j.mtbio.2021.100176.
[84] M. Murariu, S. Benali, Y. Paint, A.-L. Dechief, O. Murariu, J.-M. Raquez, P. Dubois, Molecules (2021), https://doi.org/10.3390/molecules26072043.
[85] J. Tengsuthiwat, S. Siengchin, R. Berényi, J. Karger-Kocsis, Ultraviolet nanosecond laser ablation behavior of silver nanoparticle and melamine–formaldehyde resin-coated short sisal fiber-modified PLA composites, J. Therm. Anal. Calorim. 132 (2018) 955–965, https://doi.org/10.1007/s10973-018-7048-7.
[86] C. Zhang, J. Wu, W. Liu, W. Zhang, C.-S. Lee, P. Wang, NIR-II xanthene dyes with structure-inherent bacterial targeting for efficient photothermal and broad-spectrum antibacterial therapy, Acta Biomater. 159 (2023) 247–258, https://doi.org/10.1016/j.actbio.2023.01.031.
[87] M. Yang, S. Qiu, E. Coy, S. Li, K. Zaleski, Y. Zhang, H. Pan, G. Wang, NIR-responsive TiO(2) biometasurfaces: toward in situ photodynamic antibacterial therapy for biomedical implants, Adv. Mater. 34 (2022), e2106314, https://doi.org/10.1002/adma.202106314.
[88] S. Huang, S. Xu, Y. Hu, X. Zhao, L. Chang, Z. Chen, X. Mei, Preparation of NIR-responsive, ROS-generating and antibacterial black phosphorus quantum dots for promoting the MRSA-infected wound healing in diabetic rats, Acta Biomater. 137 (2022) 199–217, https://doi.org/10.1016/j.actbio.2021.10.008.
[89] Z.-Y. Zhang, Y.-L. An, X.-S. Wang, L.-Y. Cui, S.-Q. Li, C.-B. Liu, Y.-H. Zou, F. Zhang, R.-C. Zeng, In vitro degradation, photo-dynamic and thermal antibacterial activities of Cu-bearing chlorophyllin-induced Ca–P coating on magnesium alloy AZ31, Bioact. Mater. 18 (2022) 284–299, https://doi.org/10.1016/j.bioactmat.2022.01.050.
[90] N. Anicic, M. Kurtjak, S. Jeverica, D. Suvorov, M. Vukomanovic, Antimicrobial polymeric composites with embedded nanotextured magnesium oxide, Polymers 13 (2021), https://doi.org/10.3390/polym13132183 (Basel).